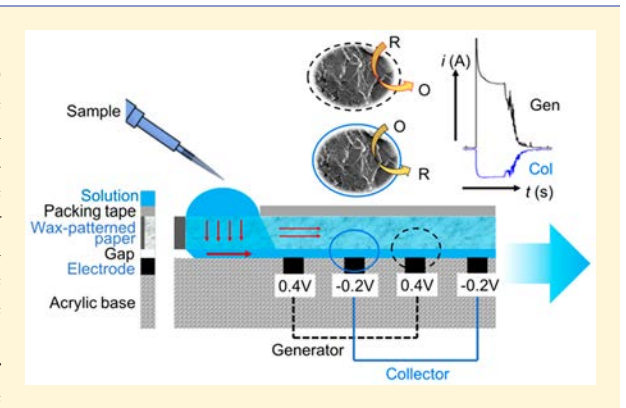


Thermoplastic Electrode Arrays in Electrochemical Paper-Based **Analytical Devices**

Eka Noviana,^{†,§} Kevin J. Klunder,[†] Robert B. Channon,[†] and Charles S. Henry^{*,†}

Supporting Information

ABSTRACT: Electrochemical paper-based analytical devices (ePADs) have garnered significant interest as an alternative to traditional benchtop methods due to their low cost and simple fabrication. Historically, ePADs have relied almost exclusively on single electrode detection, limiting potential gains in sensitivity and selectivity achievable with multiple electrodes. Herein we describe incorporation of thermoplastic electrode (TPE) arrays into flow ePADs. Quasi-steady flow was solely generated by capillary action through a fan-shaped paper device. The electrode arrays were fabricated using a simple solvent-assisted method with inexpensive materials (i.e., graphite and thermoplastic binder). These electrodes can be employed as an array of individually addressable detectors or connected as an interdigitated electrode array. The TPEs were



characterized through SEM, optical profilometry and cyclic voltammetry. Chronoamperometry was used to characterize the flow-based TPE-ePADs. Trace detection of a ferrocene complex (FcTMA⁺) was demonstrated through generation-collection experiments, achieving a limit of detection of 0.32 pmol. These TPE arrays containing ePADs show great promise as a rapid, sensitive, and low-cost sensor for point-of-need (PON) applications.

paper has been used as a platform in analytical measurement since the early 1800s and has received significant recent attention as a substrate for microfluidic devices. 1,2 Microfluidic paper-based analytical devices (µPADs) are lowcost, have a high surface area to volume ratio for chemical reaction and detection, facilitate reagent storage within the fiber network, and provide fluid transport through capillary action.^{3,4} µPADs are also amenable to modifications (e.g., biomolecule attachment, electrode incorporation, and coupling with external power source), making assays on paper tunable to achieve a required sensitivity, selectivity, and analysis time for different applications. 5-7 Various μ PADs have been reported to date for point-of-need (PON) applications featuring colorimetric or electrochemical detection. While colorimetric detection provides an easy signal readout, allowing for instrument-free measurements, 10,11 colorimetric μPADs often suffer from poor detection limits, limiting their PON use. 12 Electrochemical detection for μ PADs (ePADs) is an attractive alternative due to its high sensitivity and tunable selectivity through choice of the electrode material, technique, potential, and incorporation of biomolecules to specifically recognize the target analyte. 13,14

There are a variety of approaches for incorporating electrodes into ePADs, with screen or stencil printing carbon and metal inks onto the paper substrate as the most common.^{7,15,16} Carbon electrodes, especially composite materials, are popular in electrochemistry due to their biocompatibility, low cost, and easy fabrication.¹⁷ Carbon composites typically feature a small exposed fractional area of carbon compared to the geometric electrode area, due to the presence of insulating components. This provides lower electrode capacitance, lower background currents and higher signal-to-noise ratios in carbon composite electrodes compared to conventional solid carbon electrodes such as glassy carbon.17

Various binders including mineral oil, wax, ionic liquids, and Nafion have been reported for carbon composite fabrication. 18-21 Thermoplastic binders such as poly(methyl methacrylate) (PMMA) and polyethylene, however, have been largely unexplored despite their great mechanical stability and ability to pattern electrodes through multiple approaches. 22,23 Thermoplastic electrodes (TPEs) are typically fabricated through radiation-induced polymerization, in situ polymerization of plastic monomers in the presence of graphite, spray coating using a solvent processed plasticgraphite mixture, or molding/casting the material. 24-26 The TPE fabrication approach used in this work was adapted from a simple solvent-assisted electrode fabrication previously reported by our group.²² However, instead of using PMMA, cyclic olefin copolymer (COC) was employed here as the

Received: November 12, 2018 Accepted: January 9, 2019 Published: January 9, 2019



Department of Chemistry, Colorado State University, Fort Collins, Colorado 80523, United States

[§]Department of Pharmaceutical Chemistry, School of Pharmacy, Universitas Gadjah Mada, Yogyakarta, Indonesia

binder to create 160 μm wide TPE bands. COC has a high purity, chemical resistance, and excellent biocompatibility, making it a good binder material for electrochemical biosensors.²⁷

To date, most ePADs reported in literature employed only a single electrode for detection, limiting potential improvements in detection sensitivity and selectivity that can be gained when using multiple electrodes. 15 Zhao and co-workers reported the use of electrode arrays in PADs, however, the electrodes were used separately for multiplexed detection.²⁸ Interdigitated electrode arrays (IDAs) can enable generation-collection (GC) experiments, where the first electrode in the array oxidizes the analyte, the second reduces it, and the process is repeated across the entire array to provide an enhanced cumulative signal. IDAs are very rarely used as low cost-PON sensors as they are limited by expensive conventional fabrication techniques, such as photolithography and chemical vapor deposition. ^{29,30} A few studies have adapted IDAs into PADs via chemical deposition and gravure printing. 31,32 However, their use was limited to resistance-based measurements, with no redox-based electrochemistry performed. Yamamoto et al. recently reported redox cyling in a paper-based device.³³ Yet, the experiment was limited to only a pair of electrodes. In this work, a new PON detection platform is designed by coupling TPE arrays, consisting of up to 8 electrodes, into a flow-based ePAD. The ePAD design is based on a previous work, where fan-shaped PAD geometries generate quasi-steady flow rates, enabling functions like flow injection analysis. 34,35 The device was tested in both generation-generation (GG) mode, where potential was held constant at all electrodes, and GC mode, where two different potentials were applied to drive redox cycling. Using the TPE-ePAD, gains in sensitivity as well as low detection limits can be achieved in a pump-free flow injection system. This platform represents an important step toward low-cost and highly sensitive sensors for PON requirements.

■ EXPERIMENTAL SECTION

Chemicals and Materials. Potassium chloride (KCl) and toluene were purchased from Fisher Scientific (New Jersey, U.S.A.). Dopamine HCl and graphite (7–11 μ m size particles) were purchased from Alfa Aesar (Massachusetts, U.S.A.). Ascorbic acid, potassium hexacyanoferrate(III) (K₃Fe(CN)₆), potassium hexacyanoferrate(II) trihydrate (K₄Fe(CN)₆), and hexane were purchased from Sigma-Aldrich. All the reagents were used as received without further purification. Ferrocenylmethyl trimethylammonium hexafluorophosphate (FcTMA⁺) was synthesized in-house following published procedures.³⁶ Whatman 1, 4, and 42 filter papers were purchased from GE Healthcare (Pittsburgh, U.S.A.). PMMA (1/8 inch thick sheet) was purchased from Plaskolite Inc. (Ohio, U.S.A.). COC film (5013F) was purchased from TOPAS (U.S.A.). Conductive silver paint was obtained from SPI Supplies (Pennsylvania, U.S.A.). Packing tape, epoxy glue, copper wire, and sand papers (240- and 1500-grit) were purchased from local stores. Water used to prepare reagent solutions was purified using a Milli-Q system ($\rho \geq 18.2 \text{ M}\Omega$)

Fabrication of TPE-ePADs. The fabrication scheme is shown in Figure 1. The TPE consists of 10 individually addressable band electrodes that can be used separately as working electrodes (WE) or shorted together in generation-generation (GG) or generation-collection (GC) formats. TPE-ePAD was constructed by attaching the wax-patterned fan-

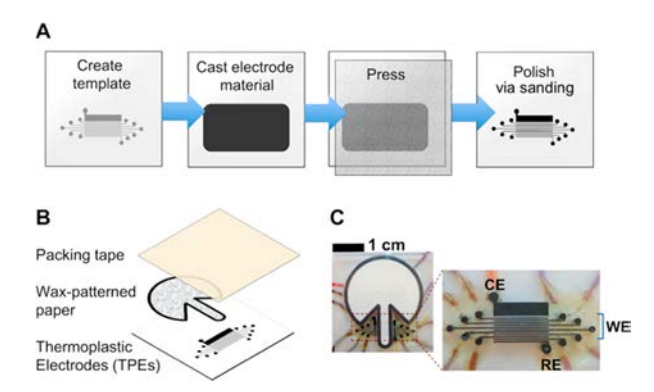


Figure 1. Schematic illustration of TPE fabrication (A) and assembly into an electrochemical PAD (B). The finished device is shown in C.

shaped filter paper onto the TPE bands using packing tape while leaving the sample inlet open to ambient air. Using this approach, the electrodes could be used many times after replacing the disposable paper devices. Detailed information on the fabrication of the electrode and paper device can be found in the Supporting Information.

Characterization of TPEs. Prior to ePAD application, the electrode material was optimized by varying the mass ratio of graphite to COC from 1:1 to 5:1. Half cm diameter test electrodes were made on PMMA substrate using these ratios. Through-plane conductivity measurements²² and cyclic voltammetry (CV) at 0.1 V/s in 0.5 KCl were carried out on the electrodes to compare the electrochemical properties. In addition, CVs of a surface insensitive (FcTMA+), a surface sensitive $(Fe(CN)_6^{3-}/Fe(CN)_6^{4-})$, and two biologically relevant redox species (dopamine and ascorbic acid) were collected on the band electrodes. A saturated calomel electrode (SCE) and TPE were used as the reference electrode (RE) and counter electrode (CE), respectively. Scan rate studies were performed by obtaining CVs at 0.01 V/s to 0.5 V/s using 5 mM FcTMA+ in 0.5 M KCl. To estimate the charge transfer rate (k_{ct}) at the electrode surface, CVs of 5 mM Fe(CN)₆^{3-/4-} in 0.5 M KCl were acquired at 0.01-0.5 V/s. Surface structure and roughness of the electrode were probed using a ISM-6500F field emission scanning electron microscope (JEOL, Tokyo, Japan) at 2 kV acceleration voltage and a ZeScope profilometer (Zemetrics, Arizona, U.S.A.), respectively.

Characterization of Flow ePADs. The ePAD was prewetted using 10 μ L of background solution (0.5 M KCl) such that the fluid front reaches the 270° wicking fan, allowing for a quasi-steady flow for the next injections. 34,35 A total of 5-25 μ L of 1 mM FcTMA⁺ solution in 0.5 M KCl was then injected onto the device inlet, and hydrodynamic amperometry was performed on one of the WE bands at 0.4 V vs carbon (C) RE. Carbon electrode was used as a pseudoreference in the array since adding a separate Ag/AgCl electrode into the flow ePAD would be difficult. Current signals at individual electrodes were monitored by amperometry during injection of 1 mM FcTMA+ solution at 0.4 V versus C using an CHI1010A potentiostat (CH Instruments, Texas, U.S.A.). Due to the capability of the potentiostat to perform only eight simultaneous measurements, we conducted the study using up to eight electrodes. To characterize and optimize the usability of the electrodes to perform redox cycling under a flow condition, several variables including the use of multiple layers of paper and different paper substrates (Whatman 1, 4 and 42), interelectrode distance and number of electrodes were tested.

Conversion and collection efficiency were calculated for each tested variable to compare their performances. Conversion efficiency was calculated as the ratio of total measured charge obtained by integrating current signal over time from an injection of 10 µL of FcTMA⁺ 1 mM to the theoretical total charge if all species injected are detected. Collection efficiency was determined by taking a ratio of total charge at the collector versus the generator during a generation-collection or redox cycling experiment. 0.4 V versus C and -0.2 V versus C were applied to the generator and collector, respectively, using a CHI1242B bipotentiostat (CH Instruments, Texas, U.S.A.). To compare sensitivity and limit of detection (LOD) of ePADs operated using a single electrode and multiple electrodes either on GG or GC mode, calibration curves were established using 5 μ L of 0.010-5.0 μ M FcTMA⁺ in 0.5 M KCl. LOD was calculated from the average plus 3× standard deviations of blank measurements in separate devices (n = 5).

■ RESULTS AND DISCUSSION

Characterization of TPEs. Electrode Morphology. The TPE IDA was first characterized through light microscopy, profilometry, and scanning electron microscopy, as shown in Figure 2. The average width of the band electrodes was found

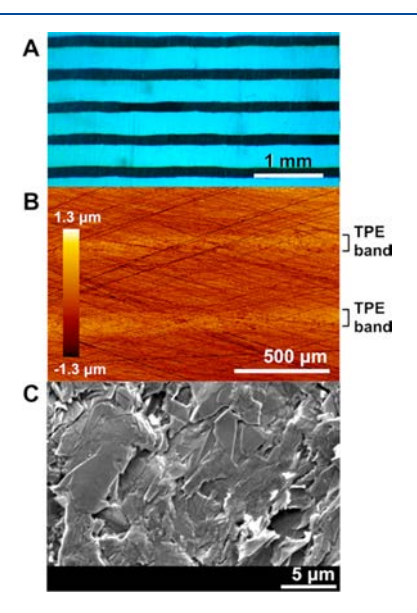


Figure 2. Surface morphology of the TPE bands imaged using (A) light microscopy, (B) profilometry, and (C) scanning electron microscopy. The electrodes were fabricated using 3:1 graphite—COC (w/w).

to be $162 \pm 11~\mu m$ (n=10) through light microscopy (Figure 2A). While smaller templates are possible based on the spot size of the laser cutter (slightly less than $100~\mu m$), smaller templates resulted in a poor mechanical stability (during sanding) and increased electrode resistance resulting in poor voltammetry. Smaller features are possible with other approaches, such as a higher resolution laser cutter or focused ion beam milling. Thowever, these fabrication techniques are more complex, time-consuming and expensive than the approach reported in this study.

The wetting properties of a material are often related to the surface roughness. When employed in a flow cell, surface roughness also affects the flow rate and the fluid dynamics (e.g., laminar or turbulent). Surface height (S_a) of the TPE

bands surface was $0.24 \pm 0.03 \mu m$ (n = 5). Water contact angles (WCA) were found to be similar between the TPE band and acrylic base surfaces, which were $65.9^{\circ} \pm 4.9^{\circ}$ and $69.0^{\circ} \pm$ 4.7°, respectively, for freshly sanded materials (Figure S1). These similar wettabilities were possibly due to mixing of materials on the surface during sanding. Similar contact angles were reported for PMMA substrate.³⁹ Li and co-workers reported static contact angle of freshly exfoliated highly ordered pyrolytic graphite (HOPG) as 64.4°.40 Average static contact angle of the TPEs increased from 65.9° to 75.7° after 1 day exposure to ambient air. This increase in contact angle was possibly due to adsorption of organic matter from air, ⁴⁰ which could be mitigated by storing the electrodes in a sealed container or resanding the surface to remove organic contaminants. After a few days of storage, the WCA of the TPEs did not change significantly (i.e., $75.1^{\circ} \pm 4.2^{\circ}$ after resanding in two consecutive days). The electrode bands were slightly more resistant to abrasion from sanding, as shown by $0.1-0.5 \mu m$ higher surfaces than those of the acrylic base (Figures 2B and S2), likely due to differences in mechanical strength between the polymeric materials.⁴¹

Scanning electron microscopy (SEM) was used to understand the surface morphology and graphitic structure (Figure 2C). Graphite sheets containing basal and edge planes are clearly visible. Slight charging on the surface was also observed due to the presence of a thin layer insulating plastic binder. Treating the surface with plasma oxidation etched out plastic from the surface, exposing more graphite while reducing surface charging (Figure S3). However, this treatment resulted in a significant growth in capacitive current (in addition to the Faradaic current), lowering the signal-to-noise ratio during electrochemical detection.

Electrochemical Behavior. As shown in Figure 3A, conductivity of the composite increased with higher graphite mass loading up to 3:1 graphite—COC (w/w), where a further increase in graphite mass percentage did not increase conductivity. A similar plateau in conductivity has been previously reported for graphite—PMMA composites above a 3:1 carbon-to-binder ratio. Conductivities of the graphite—COC composites were lower than the previously reported graphite—PMMA composites at similar ratios due to the higher electrical resistivity of the COC material. However, the average conductivity for the 3:1 graphite—COC (w/w) composite was considerably higher than that of screen-printed carbon electrodes (<10 S/m) typically employed in ePADs. 7,42

Cyclic voltammetry in 0.5 M KCl solution (Figure 3B) revealed approximately 2.8 V solvent window for the lowest graphite mass loading (1:1 w/w). The onset potential for hydrogen evolution and water oxidation decreased as the amount of graphite within the composite increased, narrowing the window significantly. Oxygen reduction peaks were observed at -1.2 V and -1.0 V versus SCE for 4:1 and 5:1 w/w of graphite to COC, respectively. This is likely due to trace metals contamination in the graphite powder (purity = 99%), as Fe, Ni, and Cu have been detected in graphite bulk material at ppm levels. We are currently investigating this matter in a concurrent study, however, it is well reported in literature that trace metals can significantly affect the electrochemical activity.

Band electrodes with $\sim 160~\mu m$ width were created using 3:1 graphite—COC and characterized before being implemented as detector arrays. Voltammetric responses of 5 mM FcTMA⁺, Fe(CN)₆^{3-/4-}, dopamine and ascorbic acid on the band

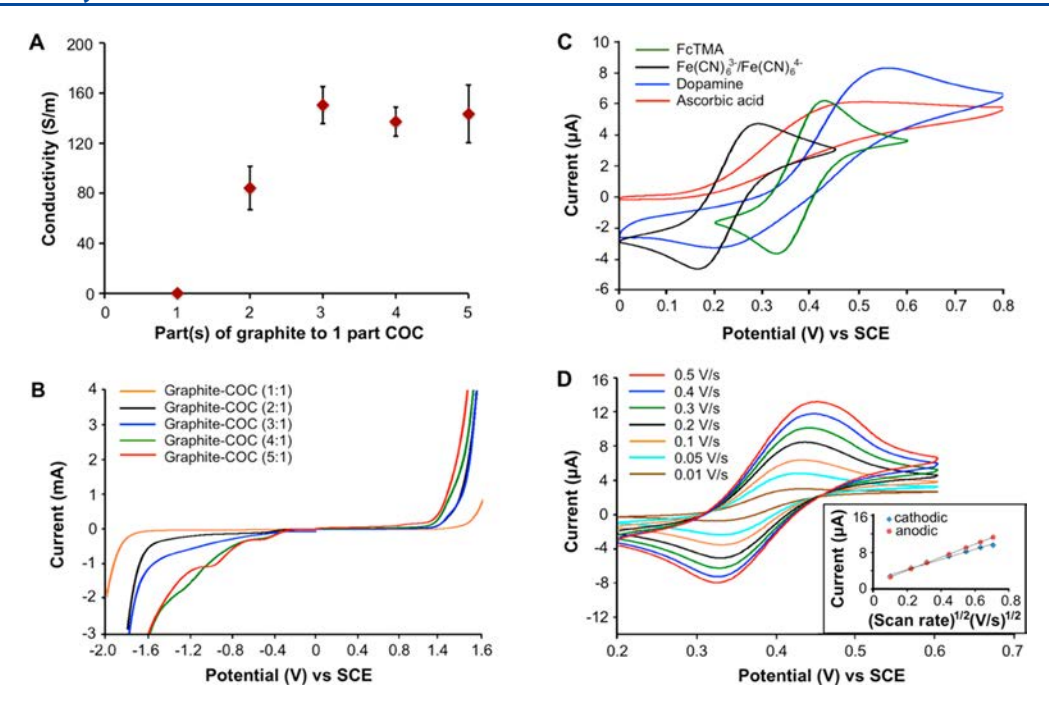


Figure 3. TPE electrochemical characterization: (A) through-plane conductivity (n = 4 electrodes, error bars indicate standard deviations) and (B) dependence of solvent window on electrode composition, (C) cyclic voltammograms of 5 mM FcTMA⁺, Fe(CN)₆³⁻/Fe(CN)₆⁴⁻, dopamine, and ascorbic acid in 0.5 M KCl, collected at 0.1 V/s on a 0.15 × 3.5 mm TPE and (D) scan rate study using 5 mM FcTMA⁺ with the resulting Randles-Sevcik plot shown in the bottom right inset.

electrode are shown in Figure 3C. Peak currents of FcTMA+ and Fe(CN)₆^{3-/4-} were close to that predicted by Randles-Sevcik equation (eq 1, predicted = $5.82 \mu A$ experimental = $6.29 \pm 0.08 \, \mu A$ and $5.59 \pm 0.05 \, \mu A$ for FcTMA⁺ and $Fe(CN)_6^{3-/4-}$, respectively). A scan rate study performed at 0.01-0.5 V/s using 5 mM FcTMA+ also gave a linear response of peak current versus $v^{1/2}$, indicative of a diffusion-controlled reaction (Figure 3D). Larger peak separations (ΔE_p) than predicted by theory were observed for these two species ($\Delta E_{\rm p}$ = 91 \pm 2 mV and 102 \pm 2 mV for FcTMA⁺ and Fe(CN)₆^{3-/4-} respectively, at 0.1 V/s). Accounting for cell resistance (1.5 k Ω by electrochemical impedance spectroscopy measurement), an 18 mV gap in peak separation resulted from the i-R drop, while the remaining may be associated with the resistance to charge transfer. The Nicholson method⁴⁵ was used to estimate the charge transfer rate (k_{ct} ; eq 2). Calculated k_{ct} were 0.004 and 0.006 cm/s for uncorrected and corrected values to cell resistance, respectively (Figure S4). These values are between the reported k_{ct} values of HOPG-basal plane ($<10^{-7}$ cm/s) and HOPG-edge plane (0.06-0.1 cm/s). Similar k_{ct} values (0.004-0.05 cm/s) for $Ru(NH_3)_6^{2+/3+})$ were previously reported on a graphene screen printed electrode, although the exact graphene loadings in the inks were not reported.⁴² Nonetheless, the charge transfer kinetic of the new composite electrodes is better than those of carbon paste electrodes (k_{ct} = $10^{-5} - 10^{-3} \text{ cm/s}$.

Sluggish electrode kinetics were observed with dopamine as exhibited by the large $\Delta E_{\rm p}$ (300 \pm 10 mV) and overpotential (390 \pm 10 mV) to drive the redox reaction. More favorable electrochemistry has previously been reported for dopamine oxidation on carbon electrodes (~150 mV vs Ag/AgCl for clean HOPG electrodes, ⁴⁷ ~180 mV vs SCE for sanded PMMA–graphite electrodes ²²). As the surface area of the band electrode was much smaller than the overall area of PMMA substrate, polishing the surface using sand paper could

potentially contaminate the electrode surface with PMMA. The PMMA film could prevent dopamine adsorption on the electrode and potentially affect the electrochemical signal. Although adsorption is not reportedly required for ascorbic acid electrochemical oxidation, the kinetics are extremely sensitive to the cleanliness of the electrode surface. ¹⁷

Electrochemical Detection in Flow ePADs. To semi-automate the sample analyses, a fan-shaped paper device was implemented in the ePAD to create quasi-steady state flow, similar to that used in traditional flow injection analyses. The 270° fan attached to the channel exit provides an expanding wicking area to increase the overall capillary pressure, counterbalancing the increase in viscous drag as the solution travels further down the channel. This results in a constant solution velocity, where straight paper channels normally exhibit decaying flow rates. 34,35,48

Figure 4A shows the amperometric response of a TPE-ePAD with 5-25 μ L injections of FcTMA⁺. A spike in current is observed immediately after droplet addition due to the high initial velocity of the flow from the small resistance encountered when displacing air with solution. The spike decays as the flow rate stabilizes, giving a current plateau, followed by a decay of current back to the baseline as the flow stops due to liquid depletion at the inlet. The magnitude of the plateau current was independent of the solution volume, suggesting that hydrostatic pressure from the solution droplet was not significant compared to capillary pressure driving the flow. The amount of detected analyte (measured as charge, mC) was linearly proportional to the amount of species of injected (Figure 4A, inset). Therefore, sample volumes as low as 5 μ L are sufficient for analytical measurements, resulting in fast analysis times (~1 min after sample injection for current to decay to baseline). Note, measurement times ranging from 7 to 20 min have been reported in previous μPADs for sub-μL injection volumes. 49,50 The proposed design can accommodate

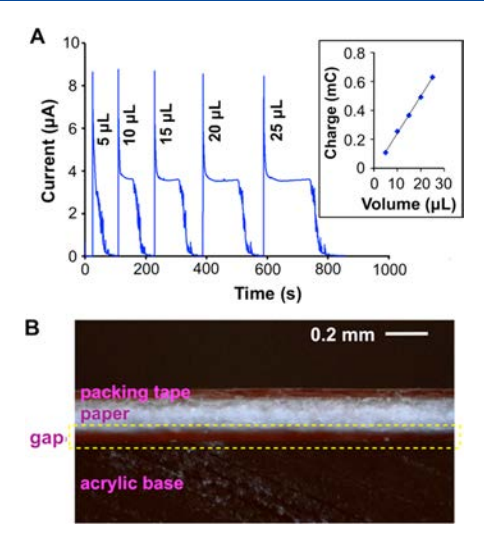


Figure 4. (A) Hydrodynamic amperogram obtained by injecting 5–25 μ L of 1 mM FcTMA⁺ in 0.5 M KCl onto an ePAD (channel width (w) = 4 mm, TPE bandwidth (x_c) = 160 μ m). Inset shows the integrated current for each injection plotted against the solution volume. (B) ePAD channel cross section during flow of a dyed solution.

up to 17 injections of 5 μ L before becoming saturated and experiencing a reduction in flow rate as well as signal (Figure S5, 5 mM FcTMA⁺ in 0.5 M KCl was used). It is also possible to increase the volume or injection capacity by increasing the size of the fan wicking portion of the device.

To characterize the fluid dynamics, the flow rate within the ePAD was estimated by imaging the flow of a solution of food dye (Figure S6). The flow rate from this dye experiment was $0.13 \pm 0.02 \ \mu L/s$, which is close to the measured flow rate from electrochemical measurements (0.11 \pm 0.02 μ L/s based on the time it took for the current signal to decay for certain injection volumes in Figure 4A). Using this experimentally determined flow rate, a theoretical plateau current was then calculated using Levich equation (eq 3) based on the geometry of the channel (assuming 150 µm paper thickness as the channel height). The theoretical plateau current was estimated to be 1.4 μ A, approximately 2.4× lower than that observed experimentally (Figure 4A). We attribute this discrepancy to the presence of a gap between the TPE-acrylic platform and the paper device, providing a lower resistance flow path compared to that through the porous network of paper. Figure 4B shows an image of the channel cross-section during solution flow, featuring a 40 \pm 10 μm channel gap. The solution imbibes into this gap and then into the paper substrate above, as shown in Figure S7. Thus, the gap serves as the main microfluidic channel, while the paper substrate sustains laminar fluid flow through capillary action (R_e < 1, eq 4). The presence of gap between two material interfaces and its contribution to the overall flow has been previously reported. 35,51,52 Assuming a channel height equal to the gap height, theoretical plateau currents are between 3.0 μ A for 50 μ m gap and 4.2 μ A for 30 μ m gap, which were in agreement to the experimental data.

Signal Generation in TPE Arrays. To assess signal generation within the electrode arrays, currents at 8 TPE bands were monitored simultaneously during a 10 μ L injection of 1 mM FcTMA⁺ (Figure 5A,B, potential = 0.4 V vs C, GG mode). A reduction in current was observed for each subsequent electrode downstream from the inlet, as expected

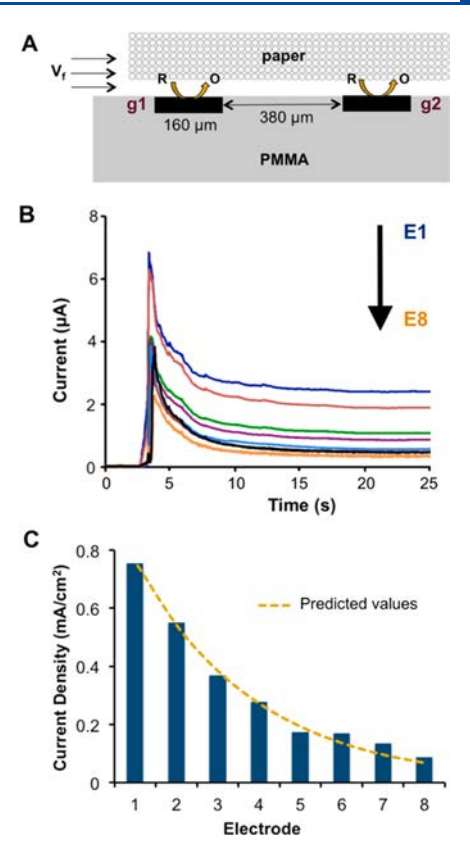


Figure 5. TPE arrays flow-ePAD under GG mode: (A) Schematic illustration of the device and redox reaction that is taking place, (B) current signals simultaneously monitored at 8 individually addressable electrodes (E1 was the closest to the inlet (upstream), w = 3 mm) from the injection of 10 μ L of 1 mM FcTMA⁺, and (C) plateau currents in B plotted against the electrode number and predicted values based on Levich and sequential regime approximation (eq 5).

for consummation of the analyte by upstream electrodes. Figure 5C shows the magnitude of plateau current normalized to the electrode area (i.e., current density) for each electrode. The ratios of current density between two adjacent electrodes ($i_{\rm g2}/i_{\rm g1}$) were approximately 74 \pm 12% (calculated by averaging ratios of current density in Figure 5C). This value was close to the 71% theoretically predicted (i.e., for $i_{\rm g1}=2.4~\mu{\rm A},~V_{\rm f}=0.087~\mu{\rm L/s})$ for a microfluidic device operated under hydrodynamic/Levich condition (eq 5). The theoretically achievable signal at the electrodes is shown as the dashed yellow line on Figure 5C.

Approximately 20% of injected redox species were turned over at the first electrode using a single layer Whatman 1 paper (Figure 6B). Under the flow condition and channel geometry, the diffusion layer thicknesses were ~15 and ~19 μ m at the center and edge of the electrode band, respectively (eq 7, Figure S8). The collection efficiency between two adjacent electrodes was 42 \pm 6%, which was higher than predicted by theory (i.e i_{g2}/i_{g1} = 29%, eq 6). While the theoretical prediction was calculated based on Levich/sequential approximation as previously described, ⁵³ the flow-ePAD may not fall within the boundary conditions for this equation wherein the predictions accurately depict the experimental results. Sequential regimes are characterized by homogeneous flow composition (i.e., no concentration gradient exists) across the microchannel before reaching second electrode. Figure S9 exhibits relationship between interelectrode distance and collection efficiency which

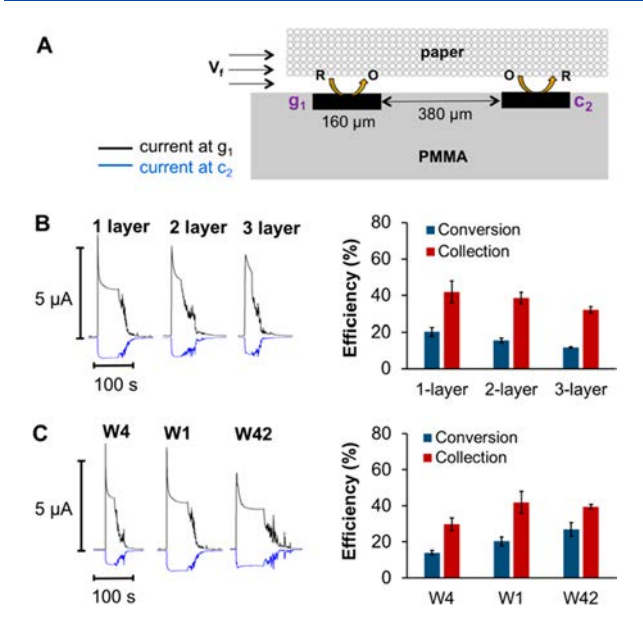


Figure 6. TPE arrays operated within flow-ePAD under GC mode experiment: schematic illustration of redox reaction that is taking place between generator (g_1) and collector (c_2) in the device (A), and conversion and collection efficiency for different number of Whatman 1 paper layer (B) and types of paper substrate (C). All these were tested using 10 μ L of 1 mM FcTMA+ (n=4 devices). Error bars indicate standard deviations. Conversion efficiencies in B and C were calculated by taking a ratio of charges measured at generator to the total theoretical charges if all analytes in the solution were electrochemically detected.

indicates that homogeneous flow composition was not achieved at electrode gaps <1.2 mm. Values close to the predicted were reported by Renault and co-workers who obtained approximately 25-30% collection efficiency using screen printed electrodes that were 2.5 mm apart and operated under similar flow velocity.⁵⁴

Modifications of ePADs and GC Performance. To adjust flow rates within the ePAD, the use of multiple layers of paper and different paper substrates as passive pumps was investigated because increases in flow rate have been reported using multiple layers of paper in μ PADs. The presence of a gap between the two sheets of paper increases the average pore radius and interstitial permeability of the paper channel to fluid flow. A 2× increase in flow rate was observed in double layer devices (Table S2), and no significant increase in volumetric flow rate was observed from double to triple layer paper devices, as has been previously observed. This could be attributed to reduction in gap heights within the triple layer device (Figure S10) since the paper layers were more tightly packed as the paper swelled.

Increased plateau currents at the generator electrode were observed as the number of paper layers increased (Figure 6B). Aside from the higher flow rates, the smaller gaps between paper and acrylic base within double and triple layer devices could reduce the effective channel height as well as the diffusive layer thickness, therefore increasing the flux of species to electrode surface. However, analyte turnover or conversion decreased in multilayer devices as the solution was distributed into a larger overall channel volume and majority of the species could not diffuse through the paper close enough to the electrode for reacting. Collection efficiency slightly went down with triple layers of paper, however, this was not statistically

different to the single- and double-layer paper devices (P = 0.05).

Another simple method to adjust the flow rates is to change the pore size of paper substrate. Whatman 1 has an approximate vertical pore diameter of 11 μ m. ⁵¹ Changing the paper to Whatman 4 (20–25 μ m vertical pore diameter) and Whatman 42 (2.5 μ m vertical pore diameter) was expected to increase and decrease flow rates, respectively. Compared to flow rates in Whatman 1, an ~33% decrease in flow rates was seen with Whatman 42 while the rates doubled in Whatman 4 (Table S2). These measured flow rates were well correlated to the experimentally observed plateau currents based on the Levich eq (Figures 6C and S11). Despite lowering the plateau currents due to reduction in analyte flux, slower flow rates provided longer time for the analyte plug to pass over the electrode. This longer residence time allowed for more analytes to diffuse down to the electrode and increased the conversion efficiency (Figure 6C). The slower flow rates in Whatman 1 and 42 (0.12 \pm 0.01 μ L/s and 0.08 \pm 0.01 μ L/s, respectively, compared to 0.24 μ L/s in Whatman 4) also improved collection efficiency of the ePAD.

Comparison of Detection Limit and Sensitivity. Figure 7A shows a comparison of generated signal (measured as total

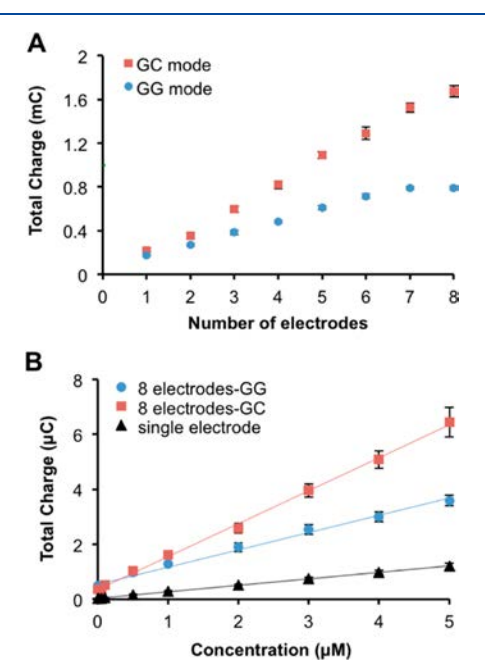


Figure 7. Signal improvement with TPE arrays: (A) total charges measured from ePAD operated with increasing number of electrodes in GG and GC modes using 1 mM FcTMA⁺ (n=4 injections), (B) calibration curves of FcTMA⁺ using single electrode (y=0.24x+0.04) and electrode arrays operated in GG (y=0.63x+0.54) and GC (y=1.20x+0.36) modes (n=4 devices). Experiments were performed using 1-layer Whatman 1, w=4 mm. Error bars indicate standard deviations.

charges) as an increasing number of TPE bands were operated together under GG and GC modes. Up to 80% of the total injected species were turned over using an array of 8 TPEs in GG mode. Based on $i_{\rm g2}/i_{\rm g1}$ that was previously determined above to be 74 \pm 12%, with approximately 18% analytes were turned over by the first electrode (g₁), the predicted total turnover for eight electrodes is between 46 and 90%. Thus, the experimental value (80% conversion) falls within the predicted

range. By employing GC mode, the achievable signal was higher than that theoretically possible without redox cycling (100% conversion = 0.96 mC) since one analyte can be turned over multiple times. Collection efficiency also increased from $39 \pm 2\%$ with 1 electrode pair to $62 \pm 1\%$ with 4 electrode pairs possibly due to the overlapping diffusion layer among electrodes (Figure S12). The total amount of signal was doubled in GC mode relative to that in GG mode when eight TPE bands were used. In addition, the trend had not yet shown an indication of signal saturation, suggesting that higher detection sensitivity can be obtained with more electrode pairs operated in GC mode.

Calibrations were established using single TPE band and TPE arrays (eight electrodes) operated in both GG and GC modes using 0.010-5.0 µM FcTMA+ (Figure 7B). Detection sensitivities were 0.24, 0.63, and 1.2 μ C/ μ M for single detector, GG arrays and GC arrays, respectively. Limits of detection (LOD) were estimated to be 90 nM for single detector, 130 nM for GG arrays and 64 nM for GC arrays (equivalent to 0.45, 0.65, and 0.32 pmol, respectively). Detection of 100 nM FcTMA+ using the 3 detection modes is shown in Figure S13. Signals from the redox analyte are visually discerned from the background signals in all three modes. However, the magnitude of signals from the GG modeoperated device could not significantly be distinguished from the background at 100 nM due to the larger noise level (Table S3). Although the detection sensitivity was improved in the electrode arrays due to higher analyte turnover, increase in electrode surface resulted in larger capacitive/background currents which limit the attainable LODs. Nonetheless, detection limits from this TPE-ePADs were considerably lower than those of previously reported direct detection ePADs which were in μ M ranges. ¹⁶/_{35,55} This low LOD of the TPEePAD was a huge improvement to make PADs more suitable for future PON applications.

CONCLUSION

Incorporation of thermoplastic electrode arrays to improve sensitivity of flow ePADs was demonstrated for the first time here. Fabrication of the electrode arrays was simple and could achieve smaller electrode size and gap compared to conventional screen-printing method. The use of inexpensive graphite and thermoplastic binders allowed for construction of electrochemical devices that cost \$1.50 per device and renewable electrodes through sanding. Increasing capillary network from the fan-shaped paper in TPE-ePADs generated a quasi-steady flow for semiautomation in analyzing multiple samples without an external pump. In addition to the rate of solution imbibition within paper substrate, the presence of gap between paper and electrode base apparently impacted flow rates within the ePADs. As the solution preferably flows through the gap rather than laterally flow through the porous substrate of the paper, the PAD devices mimic the conventional single channel-microfluidic devices. Analyte turnover was improved from 18% in single electrode detection to 80% in electrode arrays consisting of eight TPE bands. Up to 62% collection efficiency was achieved in generation-collection experiment using similar number of electrodes. Despite simpler fabrication method, collection efficiency of the TPE-ePADs was comparable to previously reported flow experiment in microfluidic devices using µm-sized IDA prepared via photolithography.56

A low limit of detection (ca. 64 nM) was attainable by the TPE-ePADs operated under GC mode. While the use of the TPE-ePAD is currently limited to analytes that are electrochemically active (electrochemically and chemically reversible for GC mode), coupling immunoassay to the TPE-ePAD will allow for the detection of various analytes ranging from small molecules to organisms such as bacteria. Many antibodies targeting these analytes are commercially available. Suitable enzyme-linked immunosorbent assay (ELISA) substrates can also be employed to generate electrochemically reversible species such as p-aminophenol (PAP) and 3,3',5,5'-tetramethylbenzidine (TMB).^{30,57} Generation of large number of detectable products from a single analyte binding event in ELISA would also improve LOD of the TPE-ePAD even further for PON applications using saliva or other sample matrices where biomarkers are present at very low concentrations (i.e., sub nM).

ASSOCIATED CONTENT

Supporting Information

The Supporting Information is available free of charge on the ACS Publications website at DOI: 10.1021/acs.analchem.8b05218.

TPE-ePAD fabrication, wettability and roughness of TPE, effect of plasma treatment, Randles-Sevcik equation, determination of charge transfer rate, determination of flow rates, Levich equation, Reynolds number, signal generation in dual band electrodes, diffusion layer thickness, dependence of collection efficiency on electrode distance and number of electrode pairs, flow rates in multilayer ePADs, comparison of signal in single and array of detector, and all equations (eqs 1–7; PDF).

AUTHOR INFORMATION

Corresponding Author

*E-mail: chuck.henry@colostate.edu.

ORCID 6

Robert B. Channon: 0000-0001-5416-7736 Charles S. Henry: 0000-0002-8671-7728

Notes

The authors declare no competing financial interest.

ACKNOWLEDGMENTS

The authors thank the United States Department of Agriculture through the National Wildlife Research Center for financial support through Grant AP17WSNWRC00C027. Additional support was provided by the National Science Foundation (1710222). We also thank Dr. Chase Gerold for acquiring profilometer image shown in Figure 2B.

REFERENCES

- (1) Crosland, M. Gay-Lussac: Scientist and Bourgeois; Cambridge University Press: Cambridge, U.K., 2004.
- (2) Martinez, A. W.; Phillips, S. T.; Butte, M. J.; Whitesides, G. M. Angew. Chem., Int. Ed. 2007, 46, 1318–1320.
- (3) Noh, H.; Phillips, S. T. Anal. Chem. 2010, 82, 4181–4187.
- (4) Fridley, G. E.; Le, H. Q.; Fu, E.; Yager, P. Lab Chip **2012**, 12, 4321–4327.
- (5) Nery, E. W.; Kubota, L. T. J. Pharm. Biomed. Anal. 2016, 117, 551–559.

- (6) Gong, M. M.; Nosrati, R.; San Gabriel, M. C.; Zini, A.; Sinton, D. J. Am. Chem. Soc. **2015**, 137, 13913–13919.
- (7) Dungchai, W.; Chailapakul, O.; Henry, C. S. Anal. Chem. 2009, 81, 5821-5826.
- (8) Martinez, A. W.; Phillips, S. T.; Carrilho, E.; Thomas, S. W.; Sindi, H.; Whitesides, G. M. Anal. Chem. 2008, 80, 3699–3707.
- (9) Hu, J.; Wang, S. Q.; Wang, L.; Li, F.; Pingguan-Murphy, B.; Lu, T. J.; Xu, F. Biosens. Bioelectron. 2014, 54, 585-597.
- (10) Zhang, Y.; Gao, D.; Fan, J.; Nie, J.; Le, S.; Zhu, W.; Yang, J.; Li, J. Biosens. Bioelectron. **2016**, 78, 538–546.
- (11) Wei, X.; Tian, T.; Jia, S.; Zhu, Z.; Ma, Y.; Sun, J.; Lin, Z.; Yang, C. J. Anal. Chem. **2016**, 88, 2345–2352.
- (12) Yang, Y.; Noviana, E.; Nguyen, M. P.; Geiss, B. J.; Dandy, D. S.; Henry, C. S. Anal. Chem. **2017**, 89, 71–91.
- (13) Zang, D.; Ge, L.; Yan, M.; Song, X.; Yu, J. Chem. Commun. 2012, 48, 4683.
- (14) Lu, J.; Ge, S.; Ge, L.; Yan, M.; Yu, J. Electrochim. Acta 2012, 80, 334-341.
- (15) Mettakoonpitak, J.; Boehle, K.; Nantaphol, S.; Teengam, P.; Adkins, J. A.; Srisa-Art, M.; Henry, C. S. *Electroanalysis* **2016**, 28, 1420–1436.
- (16) Nie, Z.; Nijhuis, C. A.; Gong, J.; Chen, X.; Kumachev, A.; Martinez, A. W.; Narovlyansky, M.; Whitesides, G. M. Lab Chip 2010, 10, 477–483.
- (17) McCreery, R. L. Chem. Rev. 2008, 108, 2646-2687.
- (18) Adams, R. N. Anal. Chem. 1958, 30, 1576.
- (19) Wang, J.; Naser, N. Anal. Chim. Acta 1995, 316, 253-259.
- (20) Liu, H.; He, P.; Li, Z.; Sun, C.; Shi, L.; Liu, Y.; Zhu, G.; Li, J. *Electrochem. Commun.* **2005**, *7*, 1357–1363.
- (21) Wang, J.; Musameh, M. Anal. Chem. 2003, 75, 2075-2079.
- (22) Klunder, K. J.; Nilsson, Z.; Sambur, J. B.; Henry, C. S. J. Am. Chem. Soc. 2017, 139, 12623-12631.
- (23) Zhong, S.; Kazacos, M.; Burford, R. P.; Skyllas-Kazacos, M. J. Power Sources 1991, 36, 29–43.
- (24) McLaren, K. G.; Batley, G. E. J. Electroanal. Chem. Interfacial Electrochem. 1977, 79, 169–178.
- (25) Yao, X.; Wu, H.; Wang, J.; Qu, S.; Chen, G. Chem. Eur. J. 2007, 13, 846-853.
- (26) Perween, M.; Parmar, D. B.; Bhadu, G. R.; Srivastava, D. N. *Analyst* **2014**, *139*, 5919–5926.
- (27) Nunes, P. S.; Ohlsson, P. D.; Ordeig, O.; Kutter, J. P. Microfluid. Nanofluid. 2010, 9, 145–161.
- (28) Zhao, C.; Thuo, M. M.; Liu, X. Sci. Technol. Adv. Mater. 2013, 14, 054402.
- (29) Goluch, E. D.; Wolfrum, B.; Singh, P. S.; Zevenbergen, M. A. G.; Lemay, S. G. Anal. Bioanal. Chem. **2009**, 394, 447–456.
- (30) Lee, G. Y.; Park, J. H.; Chang, Y. W.; Cho, S.; Kang, M. J.; Pyun, J. C. ACS Sensors **2018**, 3, 106–112.
- (31) Gartia, M. R.; Misra, S. K.; Ye, M.; Schwartz-Duval, A.; Plucinski, L.; Zhou, X.; Kellner, D.; Labriola, L. T.; Pan, D. *Sci. Rep.* **2015**, *5*, 1–15.
- (32) Zhang, J.; Huang, L.; Lin, Y.; Chen, L.; Zeng, Z.; Shen, L.; Chen, Q.; Shi, W. Appl. Phys. Lett. 2015, 106, 1-5.
- (33) Yamamoto, S.; Uno, S. Sensors 2018, 18, 730.
- (34) Mendez, S.; Fenton, E. M.; Gallegos, G. R.; Petsev, D. N.; Sibbett, S. S.; Stone, H. A.; Zhang, Y.; López, G. P. *Langmuir* **2010**, 26, 1380–1385.
- (35) Adkins, J. A.; Noviana, E.; Henry, C. S. Anal. Chem. 2016, 88, 10639–10647.
- (36) Lemay, S. G.; Van Den Broek, D. M.; Storm, A. J.; Krapf, D.; Smeets, R. M. M.; Heering, H. A.; Dekker, C. *Anal. Chem.* **2005**, *77*, 1911–1915.
- (37) Lanyon, Y. H.; De Marzi, G.; Watson, Y. E.; Quinn, A. J.; Gleeson, J. P.; Redmond, G.; Arrigan, D. W. M. *Anal. Chem.* **2007**, *79*, 3048–3055.
- (38) Taylor, J. B.; Carrano, A. L.; Kandlikar, S. G. *Int. J. Therm. Sci.* **2006**, *45*, 962–968.
- (39) Busscher, H. J.; van Pelt, A. W. J.; de Boer, P.; de Jong, H. P.; Arends, J. Colloids Surf. 1984, 9, 319–331.

(40) Li, Z.; Wang, Y.; Kozbial, A.; Shenoy, G.; Zhou, F.; McGinley, R.; Ireland, P.; Morganstein, B.; Kunkel, A.; Surwade, S. P.; Li, L.; Liu, H. *Nat. Mater.* **2013**, *12*, 925–931.

- (41) Lamonte, R. R.; McNally, D. Adv. Mater. Process. 2001, 159, 33-36.
- (42) Randviir, E. P.; Brownson, D. A. C.; Metters, J. P.; Kadara, R. O.; Banks, C. E. *Phys. Chem. Chem. Phys.* **2014**, *16*, 4598.
- (43) Ambrosi, A.; Chua, C. K.; Khezri, B.; Sofer, Z.; Webster, R. D.; Pumera, M. Proc. Natl. Acad. Sci. U. S. A. 2012, 109, 12899–12904.
- (44) Masa, J.; Zhao, A.; Xia, W.; Sun, Z.; Mei, B.; Muhler, M.; Schuhmann, W. Electrochem. Commun. 2013, 34, 113-116.
- (45) Nicholson, R. S. Anal. Chem. 1965, 37, 1351-1355.
- (46) Rice, M. E.; Galus, Z.; Adams, R. N. J. Electroanal. Chem. Interfacial Electrochem. 1983, 143, 89–102.
- (47) Patel, A. N.; Tan, S. Y.; Miller, T. S.; MacPherson, J. V.; Unwin, P. R. Anal. Chem. **2013**, *85*, 11755–11764.
- (48) Washburn, E. W. Phys. Rev. 1921, 17, 273-283.
- (49) Lankelma, J.; Nie, Z.; Carrilho, E.; Whitesides, G. M. Anal. Chem. 2012, 84, 4147–4152.
- (50) Dossi, N.; Toniolo, R.; Pizzariello, A.; Impellizzieri, F.; Piccin, E.; Bontempelli, G. *Electrophoresis* **2013**, *34*, 2085–2091.
- (51) Channon, R. B.; Nguyen, M.; Scorzelli, A.; Henry, E.; Volckens, J.; Dandy, D.; Henry, C. *Lab Chip* **2018**, *18*, 793–802.
- (52) Camplisson, C. K.; Schilling, K. M.; Pedrotti, W. L.; Stone, H. A.; Martinez, A. W. Lab Chip **2015**, *15*, 4461–4466.
- (53) Amatore, C.; Da Mota, N.; Lemmer, C.; Pebay, C.; Sella, C.; Thouin, L. Anal. Chem. **2008**, 80, 9483–9490.
- (54) Renault, C.; Anderson, M. J.; Crooks, R. M. J. Am. Chem. Soc. **2014**, 136, 4616–4623.
- (55) Santhiago, M.; Wydallis, J. B.; Kubota, L. T.; Henry, C. S. Anal. Chem. **2013**, 85, 5233–5239.
- (56) Bjorefors, F.; Strandman, C.; Nyholm, L. Electroanalysis 2000, 12, 255-261.
- (57) Niwa, O.; Xu, Y.; Halsall, H. B.; Heineman, W. R. Anal. Chem. 1993, 65, 1559–1563.